Understanding the Importance of Labile Fe(III) during Fe(II)-Catalyzed Transformation of Metastable Iron Oxyhydroxides

Juan Liu,* Anxu Sheng,* Xiaoxu Li, Yuji Arai, Yuefei Ding, Mingjun Nie, Mingquan Yan, and Kevin M. Rosso

ABSTRACT: Transformation of metastable Fe(III) oxyhydroxides is a prominent process in natural environments and can be significantly accelerated by the coexisting aqueous Fe(II) ($Fe(II)_{aq}$). Recent evidence points to the solution mass transfer of labile Fe(III) ($Fe(III)_{labile}$) as the primary intermediate species of general importance. However, a mechanistic aspect that remains unclear is the dependence of phase outcomes on the identity of the metastable Fe(III) oxyhydroxide precursor. Here, we compared the coupled evolution of Fe(II) species, solid phases, and $Fe(III)_{labile}$ throughout the Fe(II)-catalyzed transformation of lepidocrocite (Lp) versus ferrihydrite (Fh) at equal Fe(III) mass loadings with 0.2−1.0 mM $Fe(II)_{aq}$ at pH = 7.0. Similar to Fh, the conversion of Lp to product phases occurs by a dissolution−reprecipitation mechanism mediated by $Fe(III)_{labile}$ that seeds the nucleation of products. Though for Fh we observed a transformation to goethite (Gt), accompanied by the transient emergence and decline of Lp, for initial Lp we observed magnetite (Mt) as the main product. A linear correlation between the formation rate of Mt and the effective supersaturation in terms of $Fe(III)_{labile}$ concentration shows that Fe(II)-induced transformation of Lp into Mt is governed by the classical nucleation theory. When Lp is replaced by equimolar Gt, Mt formation is suppressed by opening a lower barrier pathway to Gt by heterogeneous nucleation and growth on the added Gt seeds. The collective findings add to the mechanistic understanding of factors governing phase selections that impact iron bioavailability, system redox potential, and the fate and transport of coupled elements.

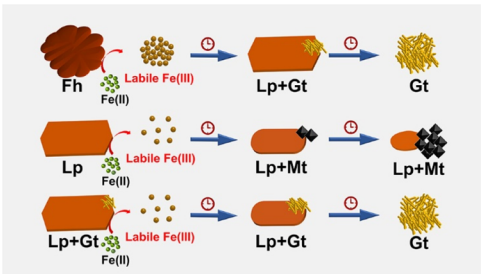

KEYWORDS: *lepidocrocite, ferrihydrite, goethite, magnetite, labile Fe(III), dissolution−reprecipitation, classical nucleation theory, heterogeneous nucleation*

INTRODUCTION

Thermodynamically metastable iron oxyhydroxides, including ferrihydrite (Fh) and lepidocrocite (Lp), are widespread in natural environments due to constantly fluctuating conditions that enable their regeneration. Example settings include soils and sediments, acid mine drainage settings, and oxidative weathering fronts.[1,2] Fh, which originates from Fe(III) hydrolysis or rapid Fe(II) oxidation, is of particular interest due to its large specific surface area and high affinity for nutrients, contaminants, and natural organic matter (NOM).[3−5] In anoxic environments at near neutral pH, coexisting aqueous Fe(II) ($Fe(II)_{aq}$), even at micromolar concentrations, can greatly accelerate Fh transformation to more stable mineral forms from years to within hours.[6,7] As one of the common intermediate product phases from this process, Lp can become persistent through cyclic redox fluctuation, particularly in environments with relatively high levels of NOM.[8−10] In addition, Lp can be readily produced from abiotic Fe(II) oxidation in excessive moisture, dissimilatory iron reduction of Fe(III) oxide, or microbial Fe(II) oxidation at circumneutral pH.[11−15] As metastable phases, both Fh and Lp will tend to ultimately transform into more stable iron oxyhydroxides, such as goethite (Gt) and hematite (Hm).[16,17] These transformations are important because by altering the mineralogy of the iron oxyhydroxides they also influence their sorption capacity, redox reactivity, and iron bioavailability controlling the mobilization/immobilization of contaminants, cycling of nutrients, and microbial extracellular respiration.[18−20]

Transformation mechanisms have been widely studied and competing pathways proposed, including dissolution−reprecipitation[21,22] and solid-state conversion.[23,24] However, tracking mass transfer of Fe(III) from precursor to product phases is a challenging task, due to the low solubility of Fe(III) at circumneutral pH, poor crystallinity, or extremely fine grain sizes of the initial mineral phases. Relative to Lp transformation, Fe(II)-catalyzed transformation of Fh has been

studied more extensively under various environmental conditions.[25−28] However, the mechanism underlying the accelerating effect of $Fe(II)_{aq}$ remains incompletely understood. It is well recognized that interfacial electron transfer (IET) can occur between sorbed Fe(II) ($Fe(II)_{sorb}$) and structural Fe(III) in Fh.[25,29] The recent isolation and quantification of an associated labile Fe(III) intermediate ($Fe(III)_{labile}$) resulting from the Fe(II)−Fh IET has provided a new framework for understanding the transformation process in terms of the classical nucleation theory (CNT).[30,31] In particular, Fe(II)-catalyzed Fh transformation kinetics and phase outcomes have now been quantified in terms of the $Fe(III)_{labile}$ saturation state. However, it remains unclear the extent to which the same mechanistic model applies to Lp as the initial precursor phase. The solubility product of Lp is ∼50 times lower than that of Fh,[32,33] suggesting that Lp is relatively more thermodynamically stable. Also, relative to Fh, Lp has a much smaller specific surface area and lower adsorption capacity for $Fe(II)_{aq}$. A key unknown is whether the accumulation rate of labile Fe(III) resulting from the IET between $Fe(II)_{sorb}$ and Lp is high enough to yield and sustain nucleation and growth of more stable product mineral phases. Moreover, in the absence of $Fe(II)_{aq}$ under ambient conditions, the spontaneous conversion of Lp to Gt is extremely slow,[34] whereas Lp production and its ultimate consumption by Gt formation were observed within 24 h during Fe(II)-catalyzed Fh transformation. How the initial metastable mineral substrate controls the transformation pathway remains poorly understood.

Previous studies specifically examining the effect of $Fe(II)_{aq}$ on Lp transformation are limited. In alkaline solution (pH = 8.5−10), Fe(II) adsorption onto Lp was found to trigger Lp transformation to Gt, magnetite (Mt), or green rust (GR), the latter two of which are mixed-valent iron oxide minerals.[35] The transformation of Lp to intermediate GR and ultimately to Mt (i.e., the Lp−GR−Mt pathway) was observed in the presence of $Fe(II)_{aq}$ and As(III)/As(V) at pH = 7.2.[36] Both Mt and GR have been widely observed as product phases from the bioreduction of Lp, but whether Mt can be directly formed from Lp bioreduction without going through the GR "step" is still under debate.[37] A variety of parameters, such as medium conditions, initial properties of Lp, supply rates of biogenic Fe(II), and bacterial activity, have been proposed to influence the final product phases of Lp bioreduction.[38−41] Hence, most prior work on this topic remains poorly interconnected and insufficient to address the question about the possibly crucial underlying importance of $Fe(III)_{labile}$ as the primary mediator of the observed phase transformations.

The objectives of this study are to: (1) investigate whether $Fe(III)_{labile}$ is produced from Fe(II)−Lp contact and, if so, assess its possible connection to the emergence of stable product phases using CNT; (2) determine how the distinct properties of Fh and Lp control the accumulation and consumption of $Fe(III)_{labile}$, as well as possibly influence the nucleation of specific product phases. We performed batch transformation experiments using equimolar ([Fe(III)]) Fh, Lp, and mixtures of Lp/Gt, in contact with 0.2−1.0 mM $FeSO_4$ solution at pH = 7.0 under anoxic conditions. The time-dependent evolution of Fe(II) species, labile Fe(III), and product phases throughout the transformation experiments were determined. Our findings reveal how the properties of metastable iron oxyhydroxides affect the accumulation rates of $Fe(III)_{labile}$ and nucleation of product phases, which provide new insights into complex transformations of iron oxyhydroxides and their implications for the sequestration and release of contaminants, NOM, and nutrients.

MATERIALS AND METHODS

Synthesis and Characterization of Iron Oxyhydroxides. Lp, 2-line Fh, and nanosized Gt particles were synthesized according to previously reported procedures.[1,22,42] More details about the preparation procedures are given in Section S1. The crystalline phase and particle size/morphology of the synthetic particles were analyzed by employing powder X-ray diffraction (XRD) and transmission electron microscopy (TEM), respectively. XRD was performed on a PANalytical X'Pert3 Powder diffractometer equipped with Cu Kα radiation (λ = 1.54056 Å) at 40 kV and 40 mA. XRD patterns were collected from 10 to 90° (2θ) with a step-size of 0.0131303° and a scan time of 44 s per step. The phases were identified using MDI Jade 6.5 software. TEM images were taken using a FEI Titan F20 microscope operated at 200 kV equipped with a Titan Themis (FEI) charge-coupled device camera and in bright-field imaging mode. Image acquisition and analysis were performed with Gatan Digital Micrograph Software. Details of sample preparation for XRD and TEM have been described in our previous studies.[9,31] The XRD patterns and representative TEM images indicate that the synthetic 2-line Fh particles had a primary particle size of 2−5 nm (Figure S1). The Lp particles were plate-like with dimensions of ∼300 nm × 100 nm and ∼15 nm thick (Figure S1), whereas Gt particles were needle-like with dimensions of ∼4 nm in width and 70 nm in length (Figure S2).

Batch Transformation Experiments. Batch transformation experiments of iron oxyhydroxides (Lp, Fh, or Lp amended with Gt) were performed using a fixed Fe(III) mass loading {[Fe(III)] = 5 mM} in 40 mL of piperazine-1,4-bisethanesulfonic acid (PIPES) solution (10 mM, pH = 7.0) with 0.2 mM, 0.4 mM, or 1.0 mM $FeSO_4$ in an anoxic glovebox. After adding the stock suspension of iron oxyhydroxides to the buffer solution, $FeSO_4$ was added to obtain the desired $[Fe(II)_{aq}]$ and initiate the transformation experiments. In the transformation experiments of Lp amended with Gt, the total Fe(III) concentration of Lp and Gt was 5 mM, and the relative molar proportion of Lp (Lp %) ranged from 40% to 100%. After vigorously mixing Lp and Gt particles in the PIPES buffer solution for more than 1 h, the $FeSO_4$ stock solution was added to initiate the transformation experiments, resulting in $[Fe(II)_{aq}]$ = 1.0 mM. Over the course of 84 h transformation experiments, the time-dependent concentrations of $Fe(II)_{aq}$, $Fe(II)_{sorb}$, and structural Fe(II) in the solid products $[Fe(II)_{stru}]$ were determined according to the procedures reported in our previous studies.[9,31] For more details about the measurements of the Fe(II) species, refer to Section S2.

Quantification of Labile Fe(III). $Fe(III)_{labile}$ in the transformation experiments was extracted and quantified as a function of time using a Fe(III)-specific complexing agent, xylenol orange disodium salt (XO, no.52097, Sigma-Aldrich) in the anoxic glovebox. XO can form colored complexes with trivalent cations, such as Fe(III), which is not disrupted by divalent cations,[43,44] so it was used to extract labile Fe(III) formed from the Fe(II)−Fh IET. The method was established and reported in our previous study.[30] Briefly, 0.9 mL of aliquots were taken at desired time intervals and vigorously mixed with 0.1 mL of the XO solution (5 mM XO and 65 mM

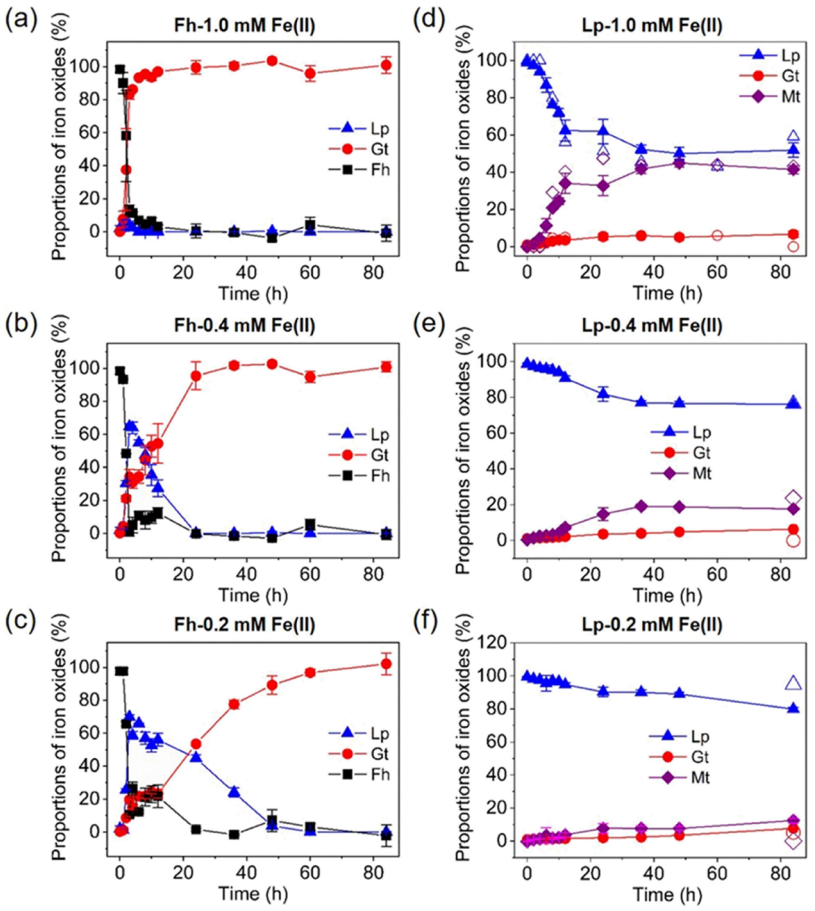

Figure 1. Time-dependent proportions of iron oxyhydroxides over the 84 h transformation experiments of ferrihydrite (Fh) (a–c) and lepidocrocite (Lp) (d–f), respectively, with 1.0 mM (a,d), 0.4 mM (b,e), and 0.2 mM (c,f) $FeSO_4$ were determined by FTIR spectroscopy. Mt and Gt stand for magnetite and goethite, respectively. Empty symbols represent the results of EXAFS, suggesting that phase proportions determined by FTIR spectroscopy are consistent with the EXAFS-based quantification.

HCl) for 20 s. The mixture was then filtered using a 0.22 μm poly(ether sulfone) filter to remove mineral particles. 160 μL of the filtrate was diluted to 2 mL using 40 mM HCl. After the sample was placed statically in the dark for 15 min to allow full color development, the concentration of $Fe(III)_{labile}$ was determined from the absorbance at 560 nm using a UV–visible spectrophotometer (Cary 100, Agilent).

Relative Proportions of Secondary Mineral Phases over Time. The relative proportions of solid phases over time were determined using attenuated total reflection Fourier transform infrared (ATR-FTIR) spectroscopy, Fe K-edge extended X-ray absorption fine structure (EXAFS) spectroscopy, and powder XRD. Details of sample preparation and parameters for data acquisition were described in our previous studies.[9,31] Aliquots were taken at intervals throughout the transformation experiments, in which the particles were collected by centrifugation and then washed with 5 mM HCl to quench phase transformation in the anoxic glovebox.[45] Samples were saved in sealed containers and taken out from the glovebox immediately before the measurements. ATR-FTIR spectra of the collected particles were obtained on a Bruker VERTEX 70 IR spectrophotometer (Bruker Optics, Ettlingen, Germany) equipped with a Bruker Platinum ATR accessory. The relative proportions of secondary mineral phases were determined from the ATR-FTIR spectra, according to a previously reported method.[31,46] As a method complementary to ATR-FTIR spectroscopy, EXAFS spectra of the end products were collected on BL12BM-B at Advanced Photon Source (Argonne, IL, USA) and beamline 4B9A at Beijing Synchrotron Radiation Facility (BSRF, Beijing, China), respectively. After spectra energy calibration, normalization, and background correction, the relative proportions of mineral phases were determined by linear combination fitting of the $k^3 \times \chi(k)$ spectra over k = 3–11 Å^{-1} with reference spectra of Fh, Lp, Gt, and Mt with the standard feature of the Athena software package.[47] The procedures for preparing and characterizing Gt and Mt standards were described in our previous study.[9]

Calculation of Nucleation Barriers for Mineral Products. To explore how the nature of the initial mineral phases (Lp vs Fh) affects the relationship between accumulation of labile Fe(III) and nucleation of product phases, we calculated the nucleation barriers for Lp, Gt, and Mt in the Fe(II)-induced transformation of Fh or Lp considering 1 μM to 10 M $FeSO_4$ at pH = 7.0. According to CNT, the nucleation barrier can be expressed as[48]

$$\Delta G^* = \frac{16\pi V_m^2 \gamma^3}{3\Delta\Psi^2} \quad (1)$$

where γ is the surface energy of the product phase (J/m^2), V_m is its volume per mol iron (cm^3/mol Fe), and $\Delta\Psi$ is the driving force for nucleation of per mole product (kJ/mol·Fe), that is the difference in the free energy (kJ/mol·Fe) of starting

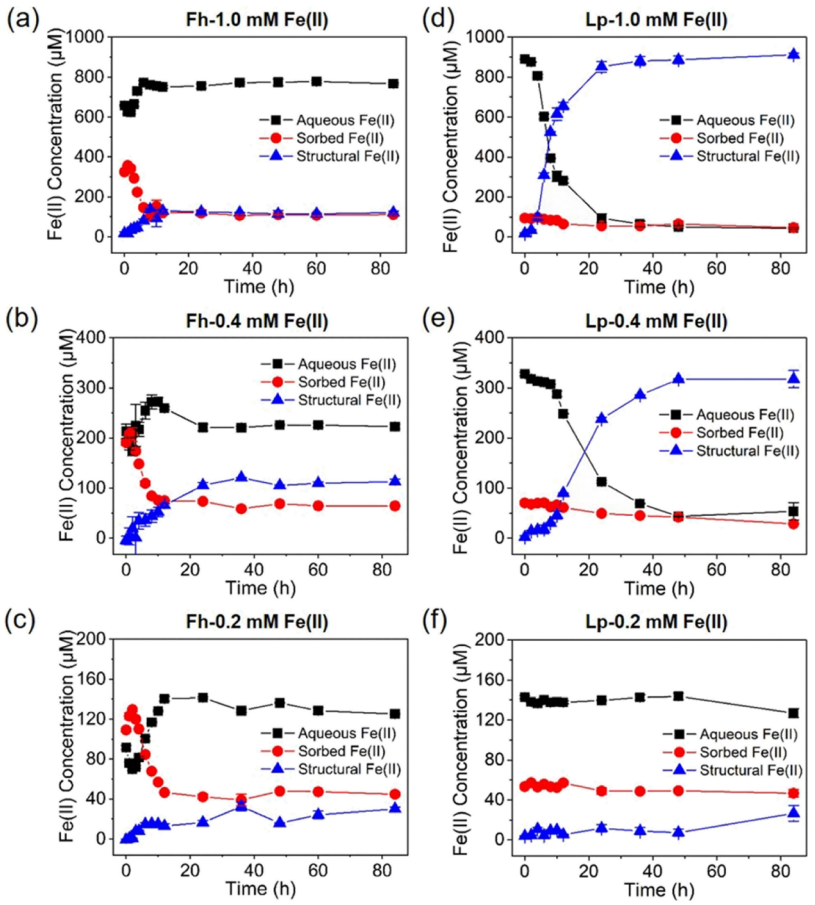

Figure 2. Time-dependent concentrations of Fe(II) species, including aqueous Fe(II) (black), sorbed Fe(II) (red), and structural Fe(II) (blue) over the 84 h experiments of Fh (a–c) and Lp (d–f) with 1.0 mM (a,d), 0.4 mM (b,e), and 0.2 mM (c,f) $FeSO_4$, respectively.

minerals (Fh/Lp) and the more stable products. The free energy of iron oxyhydroxides (Ψ) under a given pH and redox potential (Eh) condition can be calculated by constructing a thermodynamic grand potential, according to a method described previously[49,50]

$$\Psi = \frac{1}{N_{Fe}}\{G - N_o \cdot \mu_{H_2O} - (2N_o - N_H)\cdot RT\ln(10)\mathrm{pH} - (2N_o - N_H)\cdot F\cdot \mathrm{Eh}\} \quad (2)$$

where G is the molar Gibbs formation free energy; N_{Fe}, N_O, and N_H are the atomic numbers of Fe, O, and H, respectively, in the formula of iron oxyhydroxide [$Fe(OH)_3$ used for Fh];[51] μ_{H_2O} is the chemical potential of water; and F is the Faraday constant. The redox potential (Eh) of solution was estimated based on the known solubility of the starting mineral (Fh/Lp) and the concentration of $Fe(II)_{aq}$ according to a previous method,[52,53] as described in Section S3. The thermodynamic parameters of iron oxyhydroxides used in this calculation for our study are summarized in Table S1.

RESULTS AND DISCUSSION

Phase Transformation of Fh versus Lp. As shown in Figure S3, Gt was the sole product phase from the 84 h transformation experiments of Fh with 0.2–1.0 mM $FeSO_4$ at pH = 7.0. When the starting mineral was changed from Fh to Lp, Mt became the main product phase, even at a $FeSO_4$ concentration as low as 0.2 mM. Only a very weak XRD peak ($2\theta = 21.2°$) assigned to Gt was observed in the end products from the Lp transformation at $[Fe(II)_{aq}]$ = 0.2 mM, and no detectable Gt was formed at $[Fe(II)_{aq}] \geq 0.4$ mM. Moreover, the control experiments without added $FeSO_4$ showed that both Lp and Fh particles remained untransformed in the buffer solution within the 84 h experiments. Thus, the presence of 0.2–1.0 mM $Fe(II)_{aq}$ greatly accelerates transformation of both Fh and Lp at pH = 7.0, but the dominant product phases are different. This result was confirmed by both ATR-FTIR (Figure S4) and EXAFS (Figure S5) spectra.

In addition to the end products, we also measured the time evolution of solid phases in the transformation experiments using ATR-FTIR spectroscopy. In the presence of 0.2–1.0 mM $Fe(II)_{aq}$, Fh completely transformed into Gt within the 84 h experiments, accompanied by initial accumulation and ultimate consumption of Lp (Figure 1a–c), consistent with previous studies conducted at near-neutral pH and with $[Fe(II)_{aq}] \leq 1$ mM.[8,9,25,31] Although the same end product Gt was observed across the 0.2–1.0 mM $FeSO_4$ experiments, the Fh conversion rate and maximum relative proportion of Lp (Lp %) showed an expected dependence on the initial $[Fe(II)_{aq}]$. For example, as the initial $[Fe(II)_{aq}]$ increased from 0.2 to 0.4 mM, the maximum Lp % decreased from 70 to 65%, and the consumption rate of Lp increased from 0.07 to 0.16 $mM\cdot h^{-1}$ (Table S2). Correspondingly, the time for the complete conversion of Lp decreased from 48 to 24 h. In contrast, the accumulation rates of Lp were similar (1.55–1.72 $mM\cdot h^{-1}$) at different initial $[Fe(II)_{aq}]$ values. Thus, the increase of initial $[Fe(II)_{aq}]$ mainly promoted the conversion of Lp to Gt rather

than the accumulation of Lp from Fh transformation. When 1.0 mM $Fe(II)_{aq}$ was added, the maximum Lp % was only ~4% at ~ 2 h and then rapidly decreased to near zero, indicating a very fast conversion of intermediate Lp to Gt at this high $[Fe(II)_{aq}]$, which nearly outcompetes its emergence entirely.

For the experiments starting from Lp as the metastable precursor, the rate and extent of transformation were generally lower, for runs at each respective $[Fe(II)_{aq}]$ than the corresponding values for Fh (Figure 1). For example, in the presence of 1.0 mM $Fe(II)_{aq}$, Fh completely transformed into Gt after 12 h, but only 49% of Lp converted into products within 84 h. As the initial $[Fe(II)_{aq}]$ was increased from 0.2 to 1.0 mM, the extent of Lp transformation clearly increased from 20 to 49%, and the relative proportion of Mt (Mt %) increased from 13 to 41% at the end of the 84 h experiments (Table S2). However, the production rate of Gt was similar at a different initial $[Fe(II)_{aq}]$. Hence, the increase of added $Fe(II)_{aq}$ in the Lp transformation mainly facilitated the conversion of Lp to Mt, rather than to Gt. This result is substantially different from what we observed in the Fe(II)-catalyzed transformation of Fh, indicating that the properties of the initial metastable phase exerts a profound influence over the condensation of the product phases.

Evolution of Fe(II) Species in the Transformation of Fh versus Lp. Time-dependent concentrations of $Fe(II)_{aq}$, $Fe(II)_{sorb}$, and $Fe(II)_{stru}$ during the transformation of Fh and Lp are shown in Figure 2. In the Fh transformation with 0.2–1.0 mM $Fe(II)_{aq}$, a nearly instantaneous uptake of $Fe(II)_{aq}$ was observed upon spiking $FeSO_4$ into the Fh suspension, due to the large specific surface area and high adsorption capacity of Fh. This stage is followed by a more gradual adsorption of $Fe(II)_{aq}$ onto Fh within the first 1 h, followed by a clear transition to the release of $Fe(II)_{sorb}$ back to solution from 1 to 6 h, until a plateau was reached. The release of Fe(II) can be attributed to the decreasing specific surface area compared to the initial Fh as stable product phases emerge. When the initial $[Fe(II)_{aq}]$ decreased to 0.2 or 0.4 mM, a similar time-dependent evolution of $[Fe(II)_{aq}]$ and $[Fe(II)_{sorb}]$ was observed, but the maximum and final values of $[Fe(II)_{sorb}]$ were generally higher with increasing initial $[Fe(II)_{aq}]$ (Table S3). The values of $[Fe(II)_{stru}]$ in all of the Fh transformation experiments were low (30–121 μM). Moreover, no Fe(II)-containing solid phases, for example Mt, could be detected using XRD (Figure S3) or FTIR spectroscopy (Figure S4).

In the transformation experiments of Lp with added $Fe(II)_{aq}$, an instantaneous uptake of $Fe(II)_{aq}$ by Lp was also observed (Figure 2d–f). However, only 9.4–26.5% of the added $Fe(II)_{aq}$ was sorbed during this initial stage, much less than the corresponding values (32.5–54.5%) for Fh (Table S3). Moreover, $[Fe(II)_{aq}]$ monotonically decreased over time, along with a continuous increase of $[Fe(II)_{stru}]$, which is consistent with the formation of Mt indicated by the XRD, FTIR spectroscopy, and EXAFS (Figures 1, S3–S5). The final $[Fe(II)_{stru}]$ at the end of the 84 h experiments increased, as more $Fe(II)_{aq}$ was added (Table S3). The result agrees well with the increasing production of Mt observed by XRD and FTIR spectroscopy for higher initial $[Fe(II)_{aq}]$ (Figures 1 and S3b). It is noteworthy that 79.5–91.1% of the added $Fe(II)_{aq}$ precipitated as Mt after the 84 h transformation of Lp, whereas a large portion (55.7–76.7%) of $Fe(II)_{aq}$ remained in solution after the Fh transformation at 0.4–1.0 mM Fe(II) (Table S3). Thus, compared to Fh, the Fe(II)-induced Lp transformation can promote the transfer of $Fe(II)_{aq}$ from solution into the structure of solid products that tend to settle out from a water column. Compared to the evolution of $[Fe(II)_{sorb}]$ during the Fh transformation, $[Fe(II)_{sorb}]$ in the experiments with Lp did not display obvious changes over time, suggesting that the specific surface area or the affinity to $Fe(II)_{aq}$ for solid products was relatively constant during transformation.

Kinetics of Labile Fe(III) Formation and Condensation. $Fe(III)_{labile}$ concentrations over time in the transformation experiments with Fh versus Lp were compared to explore their connection to the different product phases formed. An essentially instantaneous formation of labile Fe(III) to similar concentrations (268–278 μM) was observed upon spiking 0.2–1.0 mM $FeSO_4$ into the Fh suspension (Figure 3a). Subsequently, the labile Fe(III) concentration

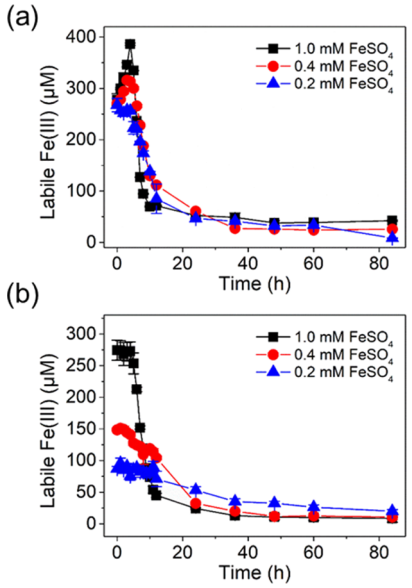

Figure 3. Time-dependent concentration of labile Fe(III) over the 84 h transformation experiments of Fh (a) and Lp (b) with 0.2 (blue), 0.4 (red), and 1.0 mM (black) $FeSO_4$, respectively.

gradually increased to its maximum at ~4 h in the experiments with 0.4–1.0 mM added $FeSO_4$, whereas no obvious change of $[Fe(III)_{labile}]$ was observed in the case with 0.2 mM $FeSO_4$. Generally, increasing amounts of added $Fe(II)_{aq}$ led to faster accumulation of $[Fe(III)_{labile}]$. After ~4 h, a rapid consumption of labile Fe(III) occurred in all cases, until reaching a plateau at $[Fe(III)_{labile}]$ = ~ 44 μM after 24 h. The time point of transition from labile Fe(III) accumulation/plateau to its rapid consumption was coincident with the emergence of product mineral phases, suggesting that the consumption of labile Fe(III) was directly related to the nucleation of product minerals. As the concentration of added $FeSO_4$ increased from 0.2 to 1.0 mM, the post-maximum consumption rate of labile Fe(III) increased from 20.5 to 79.1 $\mu M \cdot h^{-1}$ (Table S4), and the formation rate of Gt increased from 0.46 to 1.89 $mM \cdot h^{-1}$ (Table S2). The transformation of Fh into Lp or Gt are two competing pathways, which is controlled by the relative rates of olation versus oxolation reactions of labile Fe(III).[9,30] The results suggest that olation of labile Fe(III) into Gt is more favorable at the relatively higher consumption rates of labile Fe(III), which is consistent with our previous studies.[30]

For the Fe(II)-induced transformation of Lp, labile Fe(III) was also tracked, reported here for the first time, which also

showed a connection between $Fe(II)_{aq}$ sorption and the emergence of product phases. As shown in Figure 3b, rapid formation of labile Fe(III) was also observed upon spiking $FeSO_4$ into the Lp suspensions. $[Fe(III)_{labile}]$ at the first time point (~2 min) increased from 87 to 274 μM, as the added $FeSO_4$ increased from 0.2 to 1.0 mM (Table S4). In contrast to the gradual increase of $[Fe(III)_{labile}]$ observed in the Fh transformation with 0.4−1.0 mM added $FeSO_4$, the $[Fe(III)_{labile}]$ values in the Lp experiments tended to remain constant before its consumption into product minerals. Subsequently, the consumption rate of $[Fe(III)_{labile}]$ was 36.5 $\mu M \cdot h^{-1}$ in the experiments with 1.0 mM added $FeSO_4$, which was 7.3 and 20.2 times higher than the values with 0.4 and 0.2 mM $FeSO_4$, respectively (Table S4). At the same time, as the consumption rate of $[Fe(III)_{labile}]$ increased, a corresponding increase in the formation rate of Mt was clearly observable (Table S2). Overall, as was the case for the Fh system, the rapid decline of $[Fe(III)_{labile}]$ in the Lp system coincided with the emergence of product minerals (Figures 1 and 3). The collective results suggest a consistent dissolution−reprecipitation mechanism controlling the transformation of both Fh and Lp, with the nucleation of stable product phase mediated by labile Fe(III).

The work presented in our previous study using isotopic tracers suggested that labile Fe(III) can be produced from the oxidation of Fe(II) sorbed on the surface of metastable Fh.[30] Different from the IET between $Fe(II)_{sorb}$ and stable iron oxyhydroxides, such as Gt and Hm, which tends to yield "stable mineral recrystallization" in which Gt and Hm provide a template for the incorporation of Fe(III) generated by the oxidation of sorbed Fe(II),[54,55] our findings suggest that metastable iron oxyhydroxides, such as Fh and Lp, lead to a more chemically labile form of Fe(III) that is able to seed the nucleation of new product phases away from original mineral surfaces. Its accumulation rate should thus depend on both the sorption capacity and the free energy for IET of the solid substrate. The instantaneous uptake of $Fe(II)_{aq}$ by Fh was 2.1−3.5 times higher than the corresponding value by Lp at the same initial $[Fe(II)_{aq}]$ and particle loading (Table S3), reflecting the much higher sorption capacity of Fh particles (i.e., 22−65 mmol Fe(II)/mol Fh > 11−19 mmol Fe(II)/mol Lp). Furthermore, the calculated Fermi level energy of Fh (6.76 eV) is higher than that of Lp (6.38 eV),[56,57] implying that sorbed Fe(II) will be more readily oxidized by Fh relative to Lp. Both characteristics are consistent with the observed higher initial concentration and accumulation rate of labile Fe(III) in the reaction of Fh with $Fe(II)_{aq}$ (Table S4 and Figure 3).

This correlation between the labile Fe(III) activity and the nature of the initial solid substrate has consequences evident in other aspects of system evolution over time. For example, during Fh transformation, the formation of Lp from Fh conversion changed to the transformation of Lp into Gt at the time point when Fh was completely consumed (Figure 1). This result indicates that the Fe(II)-induced transformation of Lp in this system is inhibited by the presence of Fh, consistent with Fh acting as the primary source of labile Fe(III), driving it to a concentration high enough to nucleate and sustain the crystallization of both Lp and Gt. Upon exhaustion of Fh, Lp becomes the solubility limiting phase of labile Fe(III), which is consumed by ongoing Gt formation ultimately at the expense of the Lp intermediate. Our previous study shows that, in the transformation of Fh with 1 mM $FeSO_4$ at pH = 7.2, the accumulation rate of Lp was three times higher than the rate of Lp dissolution back to labile Fe(III).[30] It is the relatively fast supply of labile Fe(III) from Fe(II)−Fh IET that enables Lp formation to initially outcompete its dissolution induced by simultaneous Fe(II)-Lp IET (Figure 1).

Testing the Role of Template-Directed Nucleation and Growth on Phase Outcomes. As shown in Figure 1, Mt is the dominant solid product from the Fe(II)-induced Lp transformation, whereas Lp tends to transform into Gt in Fe(II)-catalyzed Fh transformation. Gt is present in the latter system, but not in the former. The different end products from Lp conversion in the Fh versus Lp systems cannot be attributed to the difference in supersaturation of the precursors for Mt precipitation because the supersaturation of the precursors with respect to Mt nucleation was in the same range in the two cases (Table S5). Moreover, the $[Fe(II)_{sorb}]/[Fe(III)_{labile}]$ ratio in both cases was often different from the stoichiometric Fe(II)/Fe(III) ratio (0.5) in Mt (Table S6). This contrasts Mt precipitation behavior observed in our previous study exploring the role of citrate, in which Mt appearance was correlated to this ratio.[9] We thus hypothesized that the presence of Gt in the Fh system facilitates nucleation of Gt, bypassing Mt formation, from labile Fe(III).

To test this hypothesis, we ran a third series of transformation experiments, in this case designed to compare the relative proportions of product phases that emerge in the Lp system as Lp is systematically replaced by Gt, using the initial Lp particles amended with 0−60% Gt nanoparticles on an equimolar Fe(III) basis. The total Fe(III) concentration of the starting iron oxyhydroxides was again fixed at 5 mM. As the relative proportion of Gt in the initial Fe(III) solids increased from 0 to 60%, the extent of Lp transformation at the end of the 84 h experiments increased from 44% to nearly 100%, along with increasing formation of Gt but suppressed production of Mt (Figure 4). To compare the tendency of

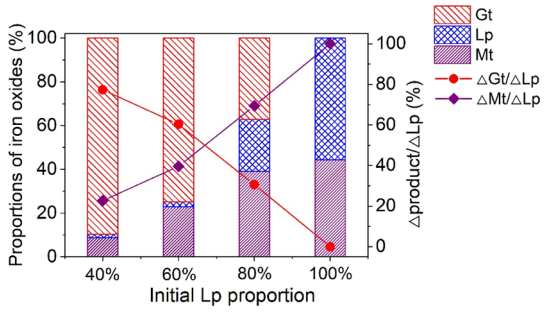

Figure 4. Relative proportions of solid phases (left *y*-axis) and the ratio of the increase in product % to the decrease in Lp %, including ΔGt/ΔLp and ΔMt/ΔLp (right *y*-axis) after the 84 h transformation of Lp with the amendment of Gt nanoparticles. The initial relative molar proportion of Lp (Lp %) was in the range of 40−100%, and the total Fe(III) concentration of Lp and Gt was fixed at 5 mM in the suspension.

Lp transformation to Gt across the experiments with the different amounts of amended Gt, we normalized the increase in the relative proportions of products against the decrease of Lp % (i.e., ΔGt/ΔLp and ΔMt/ΔLp). As the initial proportion of amended Gt increased from 0 to 60%, ΔGt/ΔLp dramatically increased from 0 to 77%, leading to the decrease of ΔMt/ΔLp from 100 to 23% (Figure 4). The results suggest that the increasing availability of Gt nanoparticles guides the

system into further Gt production and inhibits the formation of Mt.

Both homogeneous and heterogeneous nucleation of labile Fe(III) may proceed in the Fe(II)-induced transformation of metastable iron oxyhydroxides, but the nucleation rate depends exponentially on the nucleation barrier which, in turn, can be changed by the presence of a solid substrate. When the interfacial energy difference between the substrate and product phases is less than that of the fluid−substrate interface, heterogeneous nucleation is more favorable.[48] The coexisting Gt particles may provide reactive surface sites that lower the nucleation barrier for labile Fe(III) and act as a template to direct the polymerization of labile Fe(III) into Gt.[48] This is conceptually consistent with the observation of Fe(II)-catalyzed recrystallization of Gt (or Hm) noted above, in that the produced labile Fe(III) is readily incorporated into the Gt (or Hm) lattice. The similar template effect of Fe(III) oxyhydroxides has been observed in the processes of Fe^{2+} oxidation in soils, showing that the formation of Gt or Hm from Fe^{2+} oxidation is more favorable in the soils enriched with these iron oxyhydroxides.[11,58,59] Further studies would be needed to investigate the detailed structural properties of iron oxyhydroxide surfaces that facilitate lower barriers and template-directed growth.

In the transformation experiments of Fh with 0.2 mM $FeSO_4$, no Mt was detected in the end products with intermediates of ~70% Lp and ~30% Gt at the Lp transition point (Figures S3−S5). However, in the transformation experiments of Lp amended with 20−40% Gt, 23−39% of Mt formation remained. This indicates that the Gt particles from Fe(II)-catalyzed Fh transformation can promote the conversion of Lp to Gt more efficiently than the synthetic Gt particles. According to CNT, the nucleation rate is exponentially dependent on the nucleation energy barrier (ΔG^*) that is proportional to a cube of the effective interfacial energy of the nuclei (eq 1). In heterogeneous nucleation, the effect of a solid substrate on the effective interfacial energy (γ_{het}) can be given by[48]

$$\gamma_{het} = \gamma_{cl} - h(\gamma_{ls} - \gamma_{cs}) \quad (3)$$

where γ_{cl}, γ_{ls}, and γ_{cs} are the interfacial energies for the nuclei−liquid, liquid−substrate, and nuclei−substrate interfaces. Thus, the surface properties of the substrate, that is Gt in this case, can affect the value of $(\gamma_{ls} - \gamma_{cs})$ and the corresponding ΔG^*. The synthetic Gt nanoparticles are ~4 nm in width × 70 nm in length (Figure S2), which may have significantly different surface properties from the Gt particles (3 nm in width × 10 nm in length[31]) formed from Fe(II)-catalyzed transformation of Fh. In addition, the former was prepared in 5 M KOH solution at 60 °C, whereas the latter was formed by the hydrolysis and nucleation of labile Fe(III) under ambient conditions. The distinct surface properties of the two kinds of Gt particles may affect their ability to promote template-directed nucleation and growth. Nonetheless, our experiments using Gt-amended Lp confirm that template-directed nucleation of Gt is likely an important underlying cause for bypassing Mt formation.

Mechanism of Mt Formation in the Fe(II)-Accelerated Transformation of Lp. The emergence of Mt in the transformation of Lp by $Fe(II)_{aq}$ coincides with the rapid consumption of $Fe(III)_{labile}$, with higher consumption rates corresponding to faster Mt formation. Moreover, TEM images (Figure 5) show that the flat facets of the as-synthesized Lp

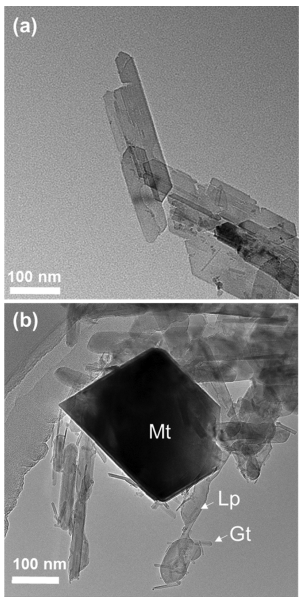

Figure 5. Representative TEM images of synthetic Lp particles before (a) and after (b) 12 h reaction with 1.0 mM $FeSO_4$ at pH = 7.0.

particles became rounded during the transformation experiments, indicating that Lp dissolution is an important component of phase evolution. The collective findings are consistent with a dissolution−reprecipitation mechanism. Although the Lp−GR−Mt pathway has been previously proposed to explain Mt formation from Lp transformation,[35,60,61] throughout our study GR was never detected.

Based on the knowledge of the time-dependent evolution of $[Fe(III)_{labile}]$ and product phases in the Fe(II)-induced transformation of Lp (Figures 1 and 3), we explored the extent to which Mt formation could be connected to $[Fe(III)_{labile}]$ in the framework of CNT. According to CNT, the nucleation rate (K) is exponentially dependent on the supersaturation (σ) of the precursor in solution[48]

$$\mathrm{Ln}\, K \propto -\frac{\gamma^3}{\sigma^2} \quad (4)$$

where γ is the interfacial free energy of the nuclei to be formed. Because Mt is mixed-valent iron oxide, $Fe(II)_{aq}$ and $Fe(II)_{sorb}$, as well as labile Fe(III), are the relevant available precursors for Mt precipitation according to

$$Fe(II)_{aq/sorb} + 2Fe(III)_{labile} + 8OH^- \Leftrightarrow Fe_3O_4 + 4H_2O \quad (5)$$

The effective supersaturation (σ_{eff}) can be estimated from the product of the precursors' activities and the activity product of reactants (K_{sp}) at equilibrium, as described by

$$\sigma_{eff} = \ln \frac{[Fe(II)_{aq} + Fe(II)_{sorb}][Fe(III)_{labile}]^2[OH^-]^8}{K_{sp}} \quad (6)$$

To explore the relationship between the formation rate of Mt and σ_{eff}, the measured $[Fe(II)_{aq}]$, $[Fe(II)_{sorb}]$, and $[Fe(III)_{labile}]$ at the emergence of Mt (2 h) were used to estimate σ_{eff}, and the initial formation rates of Mt (K_{Mt}) were obtained from the time-dependent evolution of solid phases (Figure 1d−f). K_{sp} of Mt at pH = 7.0 ($K_{sp} = [Fe^{2+}][Fe^{3+}]^2[OH^-]^8 = 10^{-108.2}$) was employed based on a previously reported value.[62]

As shown in Figure 6a, the natural logarithm of K_{Mt} exhibited a clear negative linear correlation with σ_{eff}^{-2} in the transformation of Lp with 0.2−1.0 mM $Fe(II)_{aq}$, indicating that Fe(II)-induced transformation of Lp into Mt is consistent with the principles of CNT and dominated by the accumulation of $Fe(III)_{labile}$. A similar linear correlation between the formation rates of Lp/Gt and the effective supersaturation of labile Fe(III) was observed in our previous work on Fe(II)-catalyzed transformation of Fh.[31] Thus, the accelerating effect of $Fe(II)_{aq}$ on the transformation of metastable iron oxyhydroxides, such as Fh and Lp, can be explained within this unifying conceptual framework, involving the oxidation of sorbed Fe(II), accumulation of $Fe(III)_{labile}$ toward a critical concentration with respect to product nuclei, and nucleation/growth of more thermodynamically stable iron oxyhydroxides.

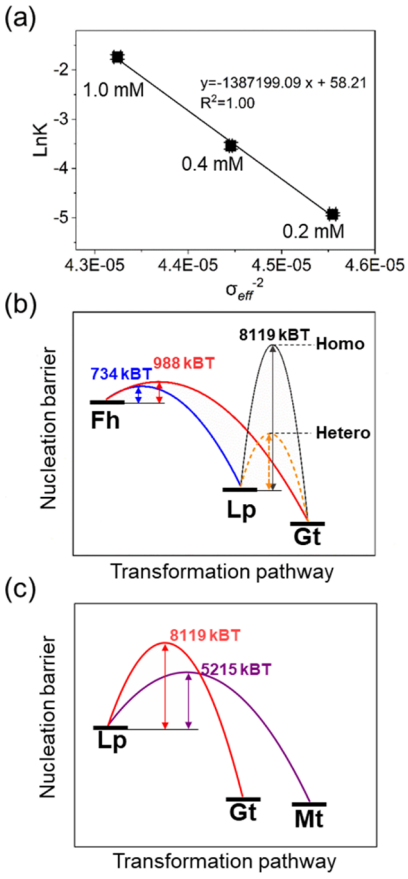

Figure 6. (a) Relationship between the initial formation rate (K) of Mt and effective supersaturation (σ_{eff}) in the Lp transformation with 0.2−1.0 mM $FeSO_4$. Transformation pathways and the nucleation barrier of products from the transformation experiments (at pH = 7 and 1.0 mM Fe(II)) with Fh (b) and Lp (c), respectively, as the starting mineral. The potential pathways for homogeneous (homo) and heterogeneous (hetero) nucleation of Gt from Lp in Fe(II)-catalyzed Fh transformation is illustrated in (b).

This framework can be extended to further verify why the nucleation of Mt is more favorable than Gt in the Fe(II)-induced transformation of Lp. To do so, we calculated the nucleation energy barrier for Mt and Gt in the transformation of Fh versus Lp across a wide range of $[Fe(II)_{aq}]$, based on the theoretical framework that combines the thermodynamic grand potential and CNT.[49,50] When two or more phases compete for the same precursors for nucleation, the phase with the lower energy barrier ($-\Delta G_c$) precipitates more rapidly. Thus, selection of the competing polymerization pathways in the Fe(II)-induced transformation of metastable iron oxyhydroxides under different conditions can be predicted according to the calculated nucleation barrier.

Figure S6 shows the nucleation energy barriers of Gt and Mt against the logarithm of initial $Fe(II)_{aq}$ concentration ($\log[Fe(II)_{aq}]$) at pH = 7.0. In the transformation of Fh with $Fe(II)_{aq}$, the nucleation energy barriers of Gt and Lp are very similar and independent of $\log[Fe(II)_{aq}]$, but that of Mt exponentially decreases with increasing $\log[Fe(II)_{aq}]$. Thus, the nucleation of Gt from Fh transformation is more favorable than Mt precipitation, until the initial $[Fe(II)_{aq}]$ increases to 114 mM or more (Figure S6). This confirms why Mt was not observed in the Fh transformation experiment with 0.2−1.0 mM added $FeSO_4$ (Figure 1). When the starting mineral is Lp and $[Fe(II)_{aq}] > 75\ \mu M$, the nucleation of Mt is favored relative to Gt (Figure S6). Thus, Mt became the dominant product phase in our Lp transformation experiments.

The energy profiles for the Fe(II)-induced transformation of Fh versus Lp with 1.0 mM added $Fe(II)_{aq}$ are shown in Figure 6b,c. In the Fh system, the nucleation energy barriers for Lp and Gt are similar and generally lower than that for Gt or Mt from Lp transformation (Figure 6b). Thus, the conversion of Lp would not occur, until Fh was completely consumed. In addition, the coexisting Gt from Fh transformation significantly lowers the nucleation energy barrier of Gt from Lp by promoting heterogeneous nucleation on Gt surface. However, the difference in the energy barrier between homogeneous and heterogeneous nucleation is unknown. Moreover, the morphology or size of Gt product from the Fe(II)-catalyzed Fh transformation clearly changes as the reaction proceeds.[63] How this morphology/size evolution of Gt nanoparticles affects their ability to promote templated conversion of Lp to Gt needs to be examined in further work. Finally, in the transformation of Lp with 1.0 mM $Fe(II)_{aq}$ at pH = 7, the nucleation energy barrier for Mt is much lower than that for Gt (Figure 6c), confirming our observation that Mt is the dominant product in the Lp system.

Environmental Implications. In natural environments, widespread metastable iron oxyhydroxides are continually undergoing slow eventual transformation into more stable minerals. Despite the environmental importance of understanding the kinetics and pathways of these transformation, mechanistic aspects that govern phase outcomes and the accelerating effect of aqueous Fe(II) have remained a matter of debate. In this study, we showed how Fe(II)-accelerated transformation of both Lp and Fh can be explained in terms of a unifying conceptual model based on $Fe(III)_{labile}$ species. Our findings also reveal how the sorption capacity for $Fe(II)_{aq}$ and the free energy for IET of metastable iron oxyhydroxides, as well as the detailed characteristics of the evolving specific surface area affect their transformation in the presence of $Fe(II)_{aq}$. Even though Mt nucleation is thermodynamically more favorable in the transformation of Lp with $Fe(II)_{aq}$ on an equimolar basis, the template-directed nucleation of Gt from labile Fe(III) consumes Lp, promoting Gt formation in the Fe(II)-catalyzed transformation of Fh. The template-directed nucleation of metastable iron oxyhydroxides could extensively occur on a variety of minerals in natural soils and sediments. Further studies are needed to investigate the mechanism and dominant factors of the template effect. The different end

products not only impact the reactive surface area, the types of elements subject to incorporation or occlusion, and iron bioavailability but also the system redox potential (Eh). The effects of environmentally relevant species, such as heavy metals, anions, and NOM, on the accumulation and consumption of labile Fe(III) and nucleation of competing product phases need to be investigated further. Moreover, further studies are needed to resolve the structure of the short-lived intermediate, labile Fe(III), such as by using advanced in situ spectroscopic techniques. This is crucial to ultimately understand the complex transformation pathways of metastable iron oxyhydroxides in natural environments.

Our findings also suggest that Fe(II)-induced transformation of Lp to Mt can be an overlooked pathway for Mt formation in natural environments. In many contexts, Mt formation is often considered a biogenic product of dissimilatory Fe(III) reduction and/or microbial Fe(II) oxidation. Our study suggested that Mt can also be formed from Lp transformation catalyzed by dissolved or biogenic Fe(II), which may impact a variety of biogeochemical processes, such as the reduction of contaminants in subsurface, microbial respiration, and direct interspecies electron transfer in syntrophic microbial communities.[64−67] The molecular mechanism presented in this study can be useful for future studies to establish interrelations among iron oxyhydroxide phase assemblages, microbial community dynamics, and contaminant fate and transport.

■ ASSOCIATED CONTENT

Supporting Information

The Supporting Information is available free of charge at https://pubs.acs.org/doi/10.1021/acs.est.1c08044.

Additional figures and details for materials and methods and results and discussion (PDF)

■ AUTHOR INFORMATION

Corresponding Authors

Juan Liu − *The Key Laboratory of Water and Sediment Sciences, College of Environmental Sciences and Engineering, Peking University, Beijing 100871, China;* orcid.org/0000-0002-8456-203X; Email: juan.liu@pku.edu.cn

Anxu Sheng − *The Key Laboratory of Water and Sediment Sciences, College of Environmental Sciences and Engineering, Peking University, Beijing 100871, China;* orcid.org/0000-0002-2050-8405; Email: shenganxu4@pku.edu.cn

Authors

Xiaoxu Li − *The Key Laboratory of Water and Sediment Sciences, College of Environmental Sciences and Engineering, Peking University, Beijing 100871, China*

Yuji Arai − *Department of Natural Resources and Environmental Sciences, University of Illinois at Urbana-Champaign, Urbana, Illinois 61801, United States;* orcid.org/0000-0002-2560-7445

Yuefei Ding − *The Key Laboratory of Water and Sediment Sciences, College of Environmental Sciences and Engineering, Peking University, Beijing 100871, China*

Mingjun Nie − *The Key Laboratory of Water and Sediment Sciences, College of Environmental Sciences and Engineering, Peking University, Beijing 100871, China*

Mingquan Yan − *The Key Laboratory of Water and Sediment Sciences, College of Environmental Sciences and Engineering, Peking University, Beijing 100871, China;* orcid.org/0000-0003-3826-0492

Kevin M. Rosso − *Pacific Northwest National Laboratory, Richland, Washington 99354, United States;* orcid.org/0000-0002-8474-7720

Complete contact information is available at: https://pubs.acs.org/10.1021/acs.est.1c08044

Notes

The authors declare no competing financial interest.

■ ACKNOWLEDGMENTS

This work was financially supported by National Natural Science Foundation of China (41820104003 and 41972318) and China National Postdoctoral Program for Innovative Talents (BX20200006). This material is also based upon the work supported by the U.S. Department of Energy, Office of Science, Office of Basic Energy Sciences, Chemical Sciences, Geosciences, and Biosciences Division through its Geosciences program at Pacific Northwest National Laboratory. This research used resources of the Advanced Photon Source, a U.S. Department of Energy (DOE) Office of Science User Facility operated for the DOE Office of Science by Argonne National Laboratory under Contract No. DE-AC02-06CH11357. We also acknowledge the support from beamline 4B9A at Beijing Synchrotron Radiation Facility (BSRF).

■ REFERENCES

(1) Cornell, R. M.; Schwertmann, U. *The Iron Oxides: Structure, Properties, Reactions, Occurences and Uses*; VCH: Weinheim, 2003, pp 1−6.

(2) Faivre, D.; Frankel, R. B. *Iron Oxides: from Nature to Applications*; John Wiley & Sons, Incorporated: Weinheim, 2016, pp 9−23.

(3) Rancourt, D. G.; Fortin, D.; Pichler, T.; Thibault, P.-J.; Lamarche, G.; Morris, R. V.; Mercier, P. H. J. Mineralogy of a natural As-rich hydrous ferric oxide coprecipitate formed by mixing of hydrothermal fluid and seawater: Implications regarding surface complexation and color banding in ferrihydrite deposits. *Am. Mineral.* **2001**, *86*, 834−851.

(4) Schwertmann, U.; Carlson, L.; Murad, E. Properties of iron oxides in two Finnish lakes in relation to the environment of their formation. *Clays Clay Miner.* **1987**, *35*, 297−304.

(5) Michel, F. M.; Ehm, L.; Antao, S. M.; Lee, P. L.; Chupas, P. J.; Liu, G.; Strongin, D. R.; Schoonen, M. A. A.; Phillips, B. L.; Parise, J. B. The structure of ferrihydrite, a nanocrystalline material. *Science* **2007**, *316*, 1726−1729.

(6) Yee, N.; Shaw, S.; Benning, L. G.; Nguyen, T. H. The rate of ferrihydrite transformation to goethite via the Fe(II) pathway. *Am. Mineral.* **2006**, *91*, 92−96.

(7) Hansel, C. M.; Benner, S. G.; Neiss, J.; Dohnalkova, A.; Kukkadapu, R. K.; Fendorf, S. Secondary mineralization pathways induced by dissimilatory iron reduction of ferrihydrite under advective flow. *Geochim. Cosmochim. Acta* **2003**, *67*, 2977−2992.

(8) Chen, C.; Kukkadapu, R.; Sparks, D. L. Influence of coprecipitated organic matter on Fe2+(aq)-catalyzed transformation of ferrihydrite: implications for carbon dynamics. *Environ. Sci. Technol.* **2015**, *49*, 10927−10936.

(9) Sheng, A.; Li, X.; Arai, Y.; Ding, Y.; Rosso, K. M.; Liu, J. Citrate controls Fe(II)-catalyzed transformation of ferrihydrite by complexation of the labile Fe(III) intermediate. *Environ. Sci. Technol.* **2020**, *54*, 7309−7319.

(10) ThomasArrigo, L. K.; Byrne, J. M.; Kappler, A.; Kretzschmar, R. Impact of Organic Matter on Iron(II)-Catalyzed Mineral Transformations in Ferrihydrite-Organic Matter Coprecipitates. *Environ. Sci. Technol.* **2018**, *52*, 12316−12326.

(11) Chen, C.; Thompson, A. Ferrous Iron Oxidation under Varying pO2 Levels: The Effect of Fe(III)/Al(III) Oxide Minerals and Organic Matter. *Environ. Sci. Technol.* **2018**, *52*, 597−606.
(12) Larese-Casanova, P.; Haderlein, S. B.; Kappler, A. Biomineralization of lepidocrocite and goethite by nitrate-reducing Fe(II)-oxidizing bacteria: Effect of pH, bicarbonate, phosphate, and humic acids. *Geochim. Cosmochim. Acta* **2010**, *74*, 3721−3734.
(13) Xiao, W.; Jones, A. M.; Li, X.; Collins, R. N.; Waite, T. D. Effect of shewanella oneidensis on the kinetics of Fe(II)-catalyzed transformation of ferrihydrite to crystalline iron oxides. *Environ. Sci. Technol.* **2018**, *52*, 114−123.
(14) Chan, C. S.; Fakra, S. C.; Emerson, D.; Fleming, E. J.; Edwards, K. J. Lithotrophic iron-oxidizing bacteria produce organic stalks to control mineral growth: implications for biosignature formation. *ISME J.* **2011**, *5*, 717−727.
(15) Liao, S.; Wang, X.; Yin, H.; Post, J. E.; Yan, Y.; Tan, W.; Huang, Q.; Liu, F.; Feng, X. Effects of Al substitution on local structure and morphology of lepidocrocite and its phosphate adsorption kinetics. *Geochim. Cosmochim. Acta* **2020**, *276*, 109−121.
(16) Bechin, K.; Šubrt, J.; Hanslik, T.; Zapletal, V.; Tláskal, J.; Lipka, J.; Sedlak, B.; Rotter, M. Transformation of synthetic gamma-FeOOH (lepidocrocite) in aqueous-solutions of ferrous sulfate. *Z. Anorg. Allg. Chem.* **1982**, *489*, 186−196.
(17) Ishikawa, T.; Takeuchi, K.; Kandori, K.; Nakayama, T. Transformation of γ-FeOOH to α-FeOOH in acidic solutions containing metal ions. *Colloids Surf., A* **2005**, *266*, 155−159.
(18) Shi, Z.; Hu, S.; Lin, J.; Liu, T.; Li, X.; Li, F. Quantifying microbially mediated kinetics of ferrihydrite transformation and arsenic reduction: role of the arsenate-reducing gene expression pattern. *Environ. Sci. Technol.* **2020**, *54*, 6621−6631.
(19) Aeppli, M.; Kaegi, R.; Kretzschmar, R.; Voegelin, A.; Hofstetter, T. B.; Sander, M. Electrochemical analysis of changes in iron oxide reducibility during abiotic ferrihydrite transformation into goethite and magnetite. *Environ. Sci. Technol.* **2019**, *53*, 3568−3578.
(20) Sun, J.; Prommer, H.; Siade, A. J.; Chillrud, S. N.; Mailloux, B. J.; Bostick, B. C. Model-Based Analysis of Arsenic Immobilization via Iron Mineral Transformation under Advective Flows. *Environ. Sci. Technol.* **2018**, *52*, 9243−9253.
(21) Hansel, C. M.; Benner, S. G.; Fendorf, S. Competing Fe(II)-induced mineralization pathways of ferrihydrite. *Environ. Sci. Technol.* **2005**, *39*, 7147−7153.
(22) Jones, A. M.; Collins, R. N.; Rose, J.; Waite, T. D. The effect of silica and natural organic matter on the Fe(II)-catalysed transformation and reactivity of Fe(III) minerals. *Geochim. Cosmochim. Acta* **2009**, *73*, 4409−4422.
(23) Burleson, D. J.; Penn, R. L. Two-step growth of goethite from ferrihydrite. *Langmuir* **2006**, *22*, 402−409.
(24) Yuwono, V. M.; Burrows, N. D.; Soltis, J. A.; Penn, R. L. Oriented aggregation: formation and transformation of mesocrystal intermediates revealed. *J. Am. Chem. Soc.* **2010**, *132*, 2163−2165.
(25) Boland, D. D.; Collins, R. N.; Miller, C. J.; Glover, C. J.; Waite, T. D. Effect of solution and solid-phase conditions on the Fe(II)-accelerated transformation of ferrihydrite to lepidocrocite and goethite. *Environ. Sci. Technol.* **2014**, *48*, 5477−5485.
(26) Zhou, Z.; Latta, D. E.; Noor, N.; Thompson, A.; Borch, T.; Scherer, M. M. Fe(II)-catalyzed transformation of organic matter-ferrihydrite coprecipitates: a closer look using Fe isotopes. *Environ. Sci. Technol.* **2018**, *52*, 11142−11150.
(27) Zhou, Z.; Muehe, E. M.; Tomaszewski, E. J.; Lezama-Pacheco, J.; Kappler, A.; Byrne, J. M. Effect of natural organic matter on the fate of cadmium during microbial ferrihydrite reduction. *Environ. Sci. Technol.* **2020**, *54*, 9445−9453.
(28) Liu, C.; Zhu, Z.; Li, F.; Liu, T.; Liao, C.; Lee, J.-J.; Shih, K.; Tao, L.; Wu, Y. Fe(II)-induced phase transformation of ferrihydrite: The inhibition effects and stabilization of divalent metal cations. *Chem. Geol.* **2016**, *444*, 110−119.
(29) Williams, A. G. B.; Scherer, M. M. Spectroscopic Evidence for Fe(II)−Fe(III) Electron Transfer at the Iron Oxide−Water Interface. *Environ. Sci. Technol.* **2004**, *38*, 4782−4790.
(30) Sheng, A.; Liu, J.; Li, X.; Qafoku, O.; Collins, R. N.; Jones, A. M.; Pearce, C. I.; Wang, C.; Ni, J.; Lu, A.; Rosso, K. M. Labile Fe(III) from sorbed Fe(II) oxidation is the key intermediate in Fe(II)-catalyzed ferrihydrite transformation. *Geochim. Cosmochim. Acta* **2020**, *272*, 105−120.
(31) Sheng, A.; Liu, J.; Li, X.; Luo, L.; Ding, Y.; Chen, C.; Zhang, X.; Wang, C.; Rosso, K. M. Labile Fe(III) supersaturation controls nucleation and properties of product phases from Fe(II)-catalyzed ferrihydrite transformation. *Geochim. Cosmochim. Acta* **2021**, *309*, 272−285.
(32) Hiemstra, T. Formation, stability, and solubility of metal oxide nanoparticles: Surface entropy, enthalpy, and free energy of ferrihydrite. *Geochim. Cosmochim. Acta* **2015**, *158*, 179−198.
(33) Navrotsky, A.; Mazeina, L.; Majzlan, J. Size-driven structural and thermodynamic complexity in iron oxides. *Science* **2008**, *319*, 1635−1638.
(34) Van Oosterhout, G. W. The transformation γ-FeO(OH) to α-FeO(OH). *J. Inorg. Nucl. Chem.* **1967**, *29*, 1235−1238.
(35) Tamaura, Y.; Saturno, M.; Yamada, K.; Katsura, T. The Transformation of γ-FeO(OH) to Fe3O4and Green Rust II in an Aqueous Solution. *Bull. Chem. Soc. Jpn.* **1984**, *57*, 2417−2421.
(36) Wang, Y.; Morin, G.; Ona-Nguema, G.; Brown, G. E., Jr. Arsenic(III) and arsenic(V) speciation during transformation of lepidocrocite to magnetite. *Environ. Sci. Technol.* **2014**, *48*, 14282−14290.
(37) Jorand, F. P. A.; Sergent, A.-S.; Remy, P.-P.; Bihannic, I.; Ghanbaja, J.; Lartiges, B.; Hanna, K.; Zegeye, A. Contribution of Anionic vs. Neutral Polymers to the Formation of Green Rust 1 from γ-FeOOH Bioreduction. *Geomicrobiol. J.* **2013**, *30*, 600−615.
(38) Zegeye, A.; Ruby, C.; Jorand, F. Kinetic and Thermodynamic Analysis During Dissimilatory γ-FeOOH Reduction: Formation of Green Rust 1 and Magnetite. *Geomicrobiol. J.* **2007**, *24*, 51−64.
(39) O'Loughlin, E. J.; Gorski, C. A.; Scherer, M. M.; Boyanov, M. I.; Kemner, K. M. Effects of Oxyanions, Natural Organic Matter, and Bacterial Cell Numbers on the Bioreduction of Lepidocrocite (γ-FeOOH) and the Formation of Secondary Mineralization Products. *Environ. Sci. Technol.* **2010**, *44*, 4570−4576.
(40) O'Loughlin, E. J.; Boyanov, M. I.; Flynn, T. M.; Gorski, C. A.; Hofmann, S. M.; McCormick, M. L.; Scherer, M. M.; Kemner, K. M. Effects of Bound Phosphate on the Bioreduction of Lepidocrocite (γ-FeOOH) and Maghemite (γ-Fe2O3) and Formation of Secondary Minerals. *Environ. Sci. Technol.* **2013**, *47*, 9157−9166.
(41) O'Loughlin, E. J.; Gorski, C. A.; Flynn, T. M.; Scherer, M. M. Electron donor utilization and secondary mineral formation during the bioreduction of lepidocrocite by shewanella putrefaciens CN32. *Minerals* **2019**, *9*, 434.
(42) Zhang, H.; Bayne, M.; Fernando, S.; Legg, B.; Zhu, M.; Penn, R. L.; Banfield, J. F. Size-dependent bandgap of nanogoethite. *J. Phys. Chem. C* **2011**, *115*, 17704−17710.
(43) Gay, C.; Collins, J.; Gebicki, J. M. Determination of Iron in Solutions with the Ferric-Xylenol Orange Complex. *Anal. Biochem.* **1999**, *273*, 143−148.
(44) Zhang, S.; Jiang, Z.; Liu, X.; Zhou, L.; Peng, W. Possible gadolinium ions leaching and MR sensitivity over-estimation in mesoporous silica-coated upconversion nanocrystals. *Nanoscale* **2013**, *5*, 8146−8155.
(45) Wu, L.; Beard, B. L.; Roden, E. E.; Johnson, C. M. Stable iron isotope fractionation between aqueous Fe(II) and hydrous ferric oxide. *Environ. Sci. Technol.* **2011**, *45*, 1847−1852.
(46) Xiao, W.; Jones, A. M.; Collins, R. N.; Bligh, M. W.; Waite, T. D. Use of fourier transform infrared spectroscopy to examine the Fe(II)-Catalyzed transformation of ferrihydrite. *Talanta* **2017**, *175*, 30−37.
(47) Ravel, B.; Newville, M. ATHENA,ARTEMIS,HEPHAESTUS: data analysis for X-ray absorption spectroscopy usingIFEFFIT. *J. Synchrotron Radiat.* **2005**, *12*, 537−541.
(48) De Yoreo, J. J.; Waychunas, G. A.; Jun, Y.-S.; Fernandez-Martinez, A. In situ investigations of carbonate nucleation on mineral and organic surfaces. *Rev. Mineral. Geochem.* **2013**, *77*, 229−257.

(49) Sun, W.; Kitchaev, D. A.; Kramer, D.; Ceder, G. Non-equilibrium crystallization pathways of manganese oxides in aqueous solution. *Nat. Commun.* **2019**, *10*, 573.
(50) Chen, B.-R.; Sun, W.; Kitchaev, D. A.; Mangum, J. S.; Thampy, V.; Garten, L. M.; Ginley, D. S.; Gorman, B. P.; Stone, K. H.; Ceder, G.; Toney, M. F.; Schelhas, L. T. Understanding crystallization pathways leading to manganese oxide polymorph formation. *Nat. Commun.* **2018**, *9*, 2553.
(51) Weatherill, J. S.; Morris, K.; Bots, P.; Stawski, T. M.; Janssen, A.; Abrahamsen, L.; Blackham, R.; Shaw, S. Ferrihydrite Formation: The Role of Fe13 Keggin Clusters. *Environ. Sci. Technol.* **2016**, *50*, 9333−9342.
(52) Stewart, S. M.; Hofstetter, T. B.; Joshi, P.; Gorski, C. A. Linking Thermodynamics to Pollutant Reduction Kinetics by Fe2+ Bound to Iron Oxides. *Environ. Sci. Technol.* **2018**, *52*, 5600−5609.
(53) Gorski, C. A.; Edwards, R.; Sander, M.; Hofstetter, T. B.; Stewart, S. M. Thermodynamic Characterization of Iron Oxide-Aqueous Fe2+ Redox Couples. *Environ. Sci. Technol.* **2016**, *50*, 8538−8547.
(54) Gorski, C. A.; Fantle, M. S. Stable mineral recrystallization in low temperature aqueous systems: A critical review. *Geochim. Cosmochim. Acta* **2017**, *198*, 439−465.
(55) Yanina, S. V.; Rosso, K. M. Linked reactivity at mineral-water interfaces through bulk crystal conduction. *Science* **2008**, *320*, 218−222.
(56) Xu, Y.; Schoonen, M. A. A. The absolute energy positions of conduction and valence bands of selected semiconducting minerals. *Am. Mineral.* **2000**, *85*, 543−556.
(57) Pearson, R. G. Absolute electronegativity and hardness: application to inorganic chemistry. *Inorg. Chem.* **1988**, *27*, 734−740.
(58) Chen, C.; Thompson, A. The influence of native soil organic matter and minerals on ferrous iron oxidation. *Geochim. Cosmochim. Acta* **2021**, *292*, 254−270.
(59) Felmy, A. R.; Moore, D. A.; Rosso, K. M.; Qafoku, O.; Rai, D.; Buck, E. C.; Ilton, E. S.; Pacific Northwest National Laboratory, R. W. A. E. M. S. L. Heterogeneous Reduction of PuO2 with Fe(II): Importance of the Fe(III) Reaction Product. *Environ. Sci. Technol.* **2011**, *45*, 3952−3958.
(60) Sumoondur, A.; Shaw, S.; Ahmed, I.; Benning, L. G. Green rust as a precursor for magnetite: an in situ synchrotron based study. *Mineral. Mag.* **2008**, *72*, 201−204.
(61) Yang, L.; Steefel, C. I.; Marcus, M. A.; Bargar, J. R. Kinetics of Fe(II)-catalyzed transformation of 6-line ferrihydrite under anaerobic flow conditions. *Environ. Sci. Technol.* **2010**, *44*, 5469−5475.
(62) Ball, J. W.; Nordstrom, D. K. *User's Manual for Wateo4f, Wtth Revised Thermodynamic Data Base and Test Cases for Calculating Speciation of Major, Trace, and Redox Elements in Natural Waters*, 1991.
(63) Qafoku, O.; Kovarik, L.; Bowden, M. E.; Nakouzi, E.; Sheng, A.; Liu, J.; Pearce, C. I.; Rosso, K. M. Nanoscale observations of Fe(II)-induced ferrihydrite transformation. *Environ. Sci.: Nano* **2020**, *7*, 2953−2967.
(64) Liu, J.; Pearce, C. I.; Liu, C.; Wang, Z.; Shi, L.; Arenholz, E.; Rosso, K. M. Fe3-xTixO4 Nanoparticles as Tunable Probes of Microbial Metal Oxidation. *J. Am. Chem. Soc.* **2013**, *135*, 8896−8907.
(65) You, Y.; Zheng, S.; Zang, H.; Liu, F.; Liu, F.; Liu, J. Stimulatory effect of magnetite on the syntrophic metabolism of Geobacter co-cultures: Influences of surface coating. *Geochim. Cosmochim. Acta* **2019**, *256*, 82−96.
(66) Liu, J.; Pearce, C. I.; Qafoku, O.; Arenholz, E.; Heald, S. M.; Rosso, K. M. Tc(VII) reduction kinetics by titanomagnetite (Fe3−xTixO4) nanoparticles. *Geochim. Cosmochim. Acta* **2012**, *92*, 67−81.
(67) Byrne, J. M.; Klueglein, N.; Pearce, C.; Rosso, K. M.; Appel, E.; Kappler, A. Redox cycling of Fe(II) and Fe(III) in magnetite by Fe-metabolizing bacteria. *Science* **2015**, *347*, 1473−1476.